AUT Journal of Electrical Engineering
10.22060/EEJ.2026.25702.5991

Ultra-Broadband and High-Efficiency Metasurface-Based Cross Polarization Converter with an Ultra-Thin Dielectric Layer for C-, X-, and Ku-Bands

SAEEDEH BARZEGAR-PARIZI,[1*]

[1]*Electrical Engineering Department, Sirjan University of Technology, Sirjan, Iran*
**Corresponding author: barzegarparizi@sirjantech.ac.ir*

Abstract— In this study, an ultra-broadband and highly efficient polarization converter based on anisotropic resonant elements is proposed and numerically analyzed. The unit cell consists of symmetrically arranged L-shaped metallic strips integrated with a central metallic circular ring, printed on a dielectric substrate and backed by a metallic ground plane with an air spacer in between. The use of an ultra-thin dielectric substrate with a thickness of 0.6 mm, combined with a 5 mm air spacer, yields a total structure thickness of approximately 5.64 mm. This multilayer arrangement enhances resonance diversity and electromagnetic coupling, thereby improving polarization conversion performance. Simulation results show that the proposed converter achieves cross-polarization conversion efficiency above 90% across the frequency range of 4.32–13.84 GHz, corresponding to a fractional bandwidth of 105%. This range covers the entire C-, X-, and Ku-bands, demonstrating the design's strong potential for multi-band applications. Analysis of the co-polarized and cross-polarized reflection coefficients reveals four distinct resonant modes arising from electric, magnetic, and hybrid resonance interactions. Together, these resonances significantly widen the operating bandwidth. In addition, the converter maintains stable performance under oblique incidence, confirming its wide-angle operation capability. Due to its compact, low-profile configuration and exceptional wideband performance, this converter is well-suited for integration into multi-band radar systems, high-gain satellite communication antennas, and advanced stealth technologies requiring broadband polarization manipulation.

Index Terms—**Cross polarization, Conversion, Efficiency, Bandwidth.**

I. INTRODUCTION

The manipulation of co-polarized and cross-polarized reflections using metasurfaces enables the realization of various electromagnetic devices, including perfect absorbers [1–4] and polarization converters. Perfect absorbers are commonly implemented using isotropic resonators, which are typically composed of arrays of symmetric metallic patterns [5,6]. Owing to their structural symmetry, these resonators exhibit strong co-polarized reflection and negligible cross-polarized reflection. When a metallic ground plane is incorporated beneath the structure, transmission is suppressed, allowing near-unity absorption to be achieved [7–9]. By introducing structural asymmetry into the resonator of a perfect absorber, polarization conversion functionality can be realized [10–13]. In such configurations, the metasurface exhibits anisotropic behavior, giving rise to significant cross-polarized reflection components [14–18]. As a result, polarization converters provide an effective means of manipulating the polarization state of incident electromagnetic waves and have attracted considerable interest for a wide range of applications [19–23].

The development of polarization converters with high conversion efficiency and broad operating bandwidth has attracted considerable attention due to their extensive applications in remote sensing, radar cross-section (RCS) reduction, and wireless communication systems [24–28]. Depending on the desired functionality, polarization converters can realize various polarization transformations, including linear-to-linear, linear-to-circular, and left-handed (right-handed) circular-

10.22060/EEJ.2026.25702.5991

to-right-handed (left-handed) circular polarization conversion [14,29,30]. Over the past few decades, conventional techniques based on the Faraday Effect, birefringence, and the optical activity of crystals have been employed to design traditional polarization converters (PCs) [31–33]. However, these approaches generally require bulky structures and large device profiles, which limit their ability to achieve broadband operation and high polarization conversion efficiency. The emergence of metasurfaces has provided an effective alternative for controlling the polarization state of electromagnetic (EM) waves while maintaining compact, lightweight, and low-profile configurations.

Metasurfaces are planar two-dimensional counterparts of metamaterials, consisting of artificially engineered periodic arrays of subwavelength metallic or dielectric elements that exhibit tailored electromagnetic responses. By properly designing the geometry and dimensions of the unit cell, metasurfaces can be engineered to realize efficient broadband polarization conversion. Based on their operating mechanism, metasurface-based polarization converters are generally classified into two categories: transmission-type and reflection-type configurations [26]. Transmission-type polarization converters often require multilayer arrangements to achieve broadband performance, resulting in increased structural complexity, larger thickness, and reduced transmission efficiency. In contrast, reflection-type polarization converters generally offer wider bandwidths and higher conversion efficiencies while maintaining relatively simple structures [26]. These advantages arise from the ability of reflective metasurfaces to support multiple resonances, which can be appropriately combined to broaden the operational bandwidth and enhance polarization conversion performance.

Several metasurface-based polarization converters have been reported in the literature. In [10], a double split-ring resonator metasurface achieved a polarization conversion ratio (PCR) exceeding 93% over the 4–14 GHz frequency range. An ultra-wideband linear polarization converter composed of a straight cut-wire and two oblique V-shaped wires was proposed in [12], providing cross-polarization efficiency above 90% from 3 to 13 GHz. In [13], a cut-square resonator loaded with circular corner rings enabled multiple polarization conversion functionalities, including linear-to-linear, linear-to-circular, and circular-to-linear conversions, with linear-to-linear operation occurring in the 6.3–6.6 GHz, 9–10.8 GHz, and 15.2–18.7 GHz bands. A single-layer anisotropic fish-like metasurface was presented in [14], exhibiting both linear cross-polarization and linear-to-circular polarization conversion with a fractional bandwidth of 31.6% (8–11 GHz). In [15], a double U-shaped metasurface achieved a conversion bandwidth of 6.91–14.31 GHz with a PCR greater than 90%. The structure reported in [17], consisting of two pairs of L-shaped metallic patches covered by a superstrate, provided efficient cross-polarization conversion with a PCR exceeding 90% over the 3.37–22.07 GHz range. Similarly, the asymmetric double-ring resonator design in [18] achieved a PCR above 90% from 6.67 to 17.1 GHz, corresponding to a relative bandwidth of 87.7%. A dual-band polarization converter employing a 45° inclined dipole-shaped metallic patch was proposed in [19], operating within the 7.1–8 GHz and 13.3–25.8 GHz frequency bands. Although these studies demonstrate significant progress in polarization conversion, achieving a combination of broad bandwidth, high conversion efficiency, low profile, and structural simplicity remains a challenging task. Furthermore, several reported wideband designs rely on multilayer metasurfaces, which increase fabrication complexity and overall thickness [22,23]. Consequently, the development of compact, ultra-thin, and broadband polarization converters continues to be an active area of research.

Hence, achieving wideband operation with high polarization conversion efficiency remains of great interest, particularly at lower frequency bands. In this paper, a simple metasurface structure composed of anisotropic resonators including a pair of L-shaped metallic strips and a central circular ring is proposed to achieve ultra-broadband and high-efficiency polarization conversion. The L-shaped strips provide anisotropy for cross-polarization conversion, while the circular ring introduces additional resonant modes and enhances electromagnetic coupling. The interaction between these elements broadens the operational bandwidth. As a result, high conversion efficiency and wide bandwidth are simultaneously achieved using a simple single-layer metasurface architecture. The physical mechanism underlying the broadband response is analyzed through electric and magnetic resonance interactions by examining the surface current distributions on the metasurface and ground plane. Simulation results demonstrate that the proposed structure achieves cross-polarization conversion with efficiency exceeding 90% over the frequency range of 4.32–13.84 GHz, corresponding to a fractional bandwidth of 105%. The operational band of 4.32–13.84 GHz covers several important microwave communication and sensing bands, including the C-band (4–8 GHz), X-band (8–12 GHz), and part of the Ku-band (12–18 GHz). These frequency ranges are widely used in satellite communications, radar systems, remote sensing, electronic warfare, and radar cross-section (RCS) reduction applications, where efficient polarization manipulation over a wide bandwidth is highly desirable. In particular, broadband cross-polarization converters operating across multiple adjacent bands can significantly enhance system robustness against polarization mismatch, enable multifunctional antenna and reflector designs, and improve performance in wideband radar and imaging systems. Therefore, achieving a polarization conversion ratio exceeding 90% over the 4.32–13.84 GHz range makes the proposed metasurface especially suitable for practical, wideband microwave application.

10.22060/EEJ.2026.25702.5991

The remainder of this paper is organized as follows. Section 2 presents the configuration of the proposed structure along with the simulation results. A mathematical discussion is provided to analyze the anisotropic characteristics of the medium and to clarify the polarization conversion mechanism. Additionally, field distributions and surface current vectors are illustrated to explain the physical mechanism responsible for the broadband behavior. Finally, Section 3 concludes the paper with the main findings.

II. Configuration

In this section, a broadband polarization converter composed of an anisotropic medium is presented. The unit cell of the proposed structure is illustrated in Fig. 1. The unit cell of the structure consists of a metasurface including one pair of L-shaped strips in combination with a metallic circular ring at the center, a dielectric substrate of RT/Duroid5880 with relative permittivity of 2.2 and thickness of h_d and an air spacer with thickness of h_s terminated by a metallic film acting as back reflector. The top and bottom layers are made of copper, with an electric conductivity of 5.96×10^7 S/m and a thickness of $t = 0.02$ mm. The period of the structure is supposed L in *x*- and *y*-directions. The geometrical parameters of the metasurface are demonstrated in Fig. 1b. The length and the width of strips are supposed *d* and *w*, respectively. L-shaped strips are placed at a distance of g from the edge of a single unit cell. The radii of the circular rings are considered R_1 and R_2.

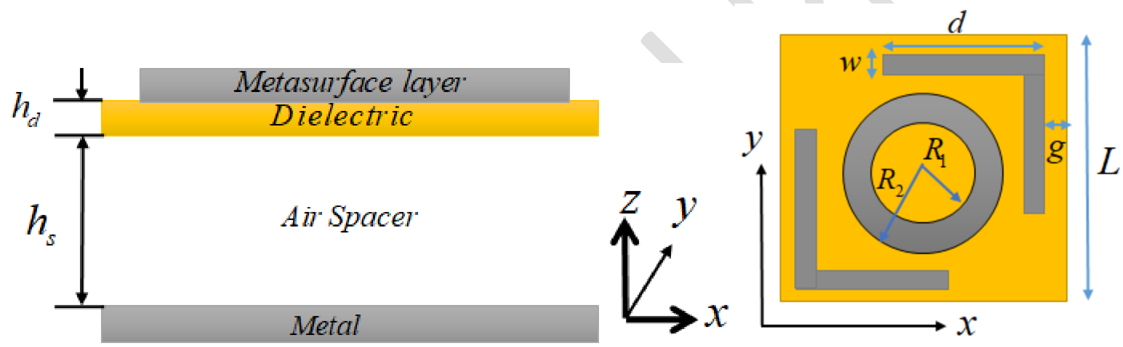

(a) (b)

Fig.1 (a) a Perspective view of unit cell geometry of the proposed structure including a single layer of the metasurface deposited on a dielectric substrate placed on a spacer and a metallic reflector at the bottom. (b)Top view of the top metasurface including one pair L-shaped strips in combination with a metallic circular ring at the center.

Initially, geometric asymmetry is introduced by incorporating L-shaped metallic strips, which induces bi-anisotropic coupling between the electric and magnetic responses. This intentional symmetry breaking enables efficient conversion of an incident linear polarization into its orthogonal state, resulting in strong cross-polarized reflection and an enhanced polarization conversion ratio (PCR). Subsequently, a central circular metallic ring is added to the unit cell to improve impedance matching between the metasurface and free space for the co-polarized component, further enhancing the PCR. Moreover, the structure supports multiple hybridized electric and magnetic resonances, which play a crucial role in realizing ultra-broadband behavior.
The proposed polarization converter can be fabricated using standard printed circuit board (PCB) technology. First, a RT/Duroid 5880 substrate is selected as the dielectric layer. The top metasurface pattern, consisting of the L-shaped metallic strips and the central circular ring, can be realized using conventional photolithography and chemical etching processes. A continuous copper sheet is employed as the ground plane. Subsequently, a low-loss dielectric spacer or mechanical supporting posts can be used to maintain the designed air-gap thickness between the substrate and the metallic reflector. Finally, the fabricated sample can be characterized in an anechoic chamber using a vector network analyzer and two linearly polarized horn antennas to measure the co-polarized and cross-polarized reflection coefficients under normal and oblique incidences.In practical implementations, fabrication tolerances, variations in substrate properties, conductor surface roughness, finite conductivity, layer misalignment, and air-gap deviations may cause slight shifts in resonance frequencies and minor degradation in polarization conversion performance. In addition, measurement uncertainties such as antenna

10.22060/EEJ.2026.25702.5991

misalignment and environmental reflections can lead to discrepancies between simulated and measured results. Nevertheless, due to the multiple coupled resonances and broadband operating mechanism, the proposed converter is expected to remain relatively robust against moderate fabrication and assembly imperfections.

The geometrical parameters shown in Fig. 1 were obtained through a systematic parametric sweep and numerical optimization process carried out in a full-wave electromagnetic simulation environment. Starting from an initial physically motivated design, key parameters such as the length of the L-shaped strips, gap spacing, and the radii of the circular ring were varied individually and in combination to evaluate their influence on resonance positions, impedance matching, and polarization conversion ratio (PCR). The final optimized dimensions were selected to maximize the PCR above 90% over the targeted ultra-broadband frequency range, while maintaining good impedance matching and stable performance. The optimized geometric parameters of the proposed structure are considered to be L = 14 mm, g = 1 mm, w = 1 mm, d = 10 mm, R_1 = 3 mm, R_2=1 mm, h_d=0.6 mm, and h_s=5 mm. The simulations were performed using HFSS, where unit-cell boundary conditions were applied along the x- and y-directions, and a Floquet port was assigned along the z-direction. Owing to the diagonal symmetry of the proposed unit cell, the results for y-polarized incidence are equivalent to those for x-polarized incidence under normal illumination. Since the structure incorporates a metallic back reflector, the transmission coefficients are zero; therefore, the analysis focuses exclusively on the reflection characteristics. The relationship between the reflected and incident linearly polarized waves can be expressed using the Jones matrix [34]:

$$\begin{pmatrix} E_r^x \\ E_r^y \end{pmatrix} = \begin{pmatrix} r_{xx} & r_{xy} \\ r_{yx} & r_{yy} \end{pmatrix} \begin{pmatrix} E_i^x \\ E_i^y \end{pmatrix} \tag{1}$$

In this equation, r_{xx} and r_{yy} are co-polarized components of the reflection, r_{xy} and r_{yx} are cross-polarized components of the reflection. The polarization direction of the waves is illustrated by the superscripts *x* and *y*, while the reflected and incident waves are demonstrated by the subscripts r and i, respectively. The y-polarized incidence is considered to analyze in this study. In addition, the reflected wave includes both cross- and co-polarized coefficients. In this case, the cross-polarized reflection coefficient is $r_{xy} = E_r^x / E_i^y$ and the co-polarized reflection coefficient is defined as $r_{yy} = E_r^y / E_i^y$.

Fig. 2(a) shows the magnitude of the co-polarized reflection coefficient (r_{yy}) and cross polarized reflection coefficient (r_{xy}). As shown in Fig. 2(a), resonance frequencies are observed at 4.64 GHz, 7.22 GHz, 11.64 GHz, and 13.65 GHz, corresponding to the dips in the co-polarized reflection coefficient. At these frequencies, the incident y-polarized wave is almost completely converted into an x-polarized wave upon reflection from the metasurface. Within the frequency range of 4.32–13.84 GHz, the co-polarized reflection component remains below 0.3, while the cross-polarized reflection component exceeds 0.94. The polarization conversion efficiency is quantified by the polarization conversion ratio (PCR), which is defined as:

$$PCR = \frac{|r_{xy}|^2}{|r_{xy}|^2 + |r_{yy}|^2} \tag{2}$$

As observed, the PCR exceeds 90% within the 4.32–13.84 GHz frequency range, indicating that the incident y-polarized wave is efficiently converted into an x-polarized wave throughout this band. The relative bandwidth (RBW) reaches approximately 105%, demonstrating the ultra-wideband nature of the proposed metasurface. The PCR value at the four resonant frequencies is unity, confirming complete polarization conversion at these points. The proposed structure achieves a minimum polarization conversion ratio (PCR) of 92% occurring at 9.6 GHz within the operating band. The broadband performance is attributed to the coupling and overlap of adjacent resonances. To gain deeper insight into the underlying mechanism, the electric and magnetic field distributions at the resonant frequencies are analyzed in the following section.

10.22060/EEJ.2026.25702.5991

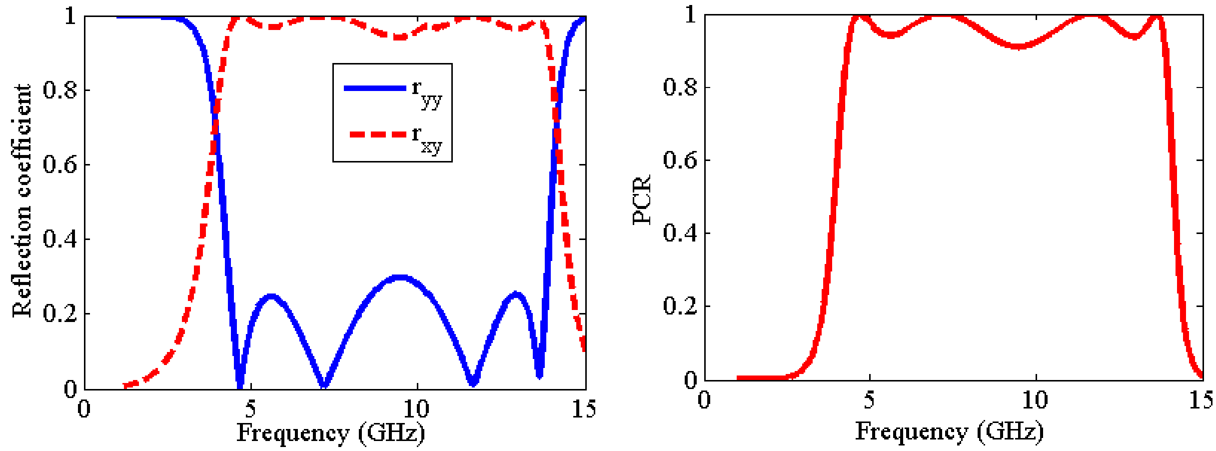

(a) (b)

Fig.2 Simulated (a) reflection coefficients (b) PCR of the proposed structure under the normal incidence

A mathematical analysis is presented to investigate the anisotropic characteristics of the medium and to provide a deeper understanding of the polarization conversion mechanism of the proposed structure [10,14,34-36]. A rotated rectangular coordinate system (u–v) is introduced, oriented at 45° relative to the original x–y axes, as illustrated in Fig. 3. The analysis is performed for a y-polarized incident wave; however, similar results are obtained for x-polarized incidence. The y-polarized incident wave can be decomposed into components along the u- and v-axes, expressed as:

$$\vec{E}_i = \hat{y}E_i^y = \hat{u}E_i^u + \hat{v}E_i^v \tag{3}$$

Where $\hat{u}$ and $\hat{v}$ are the unit vectors along *u*- and *v*-axis; $E_i^u = E_i^v = 0.707E_i^y$. The reflected electric field can be written as:

$$\vec{E}_r = \hat{u}E_r^u + \hat{v}E_r^v = \hat{u}\left(r_{uu}E_i^u e^{i\Phi_{uu}} + r_{uv}E_i^v e^{i\Phi_{uv}}\right) + \hat{v}\left(r_{vu}E_i^u e^{i\Phi_{vu}} + r_{vv}E_i^v e^{i\Phi_{vv}}\right) \tag{4}$$

where r_{uu}, Φ_{uu} and r_{vv}, Φ_{vv} are the amplitude and phase of co-polarized reflection coefficients for *u*-to-*u* and *v*-to-*v* polarization conversion, respectively; r_{vu}, Φ_{vu} and r_{uv}, Φ_{uv} are the amplitude and phase of cross-polarized reflection coefficients for *u*-to-*v* and *v*-to-*u* polarization conversion, respectively. Since the proposed structure is asymmetric, it shows anisotropic properties with dispersive relative permittivity and permeability. Hence, there is a difference in the phase and the amplitude of the reflection waves in *u*- and *v*-components. If $r_{uu} = r_{vv} \approx 1$, $r_{uv} = r_{vu} \approx 0$, Eq. (4) appears as:

$$\vec{E}_r = \hat{u}E_i^u e^{i\Phi_{uu}} + \hat{v}E_i^v e^{i\Phi_{vv}} \tag{5}$$

The incident and the reflected electric field must satisfy $\vec{E}_i.\vec{E}_r = 0$, in order to be perpendicular to each other. This condition leads to the below relation:

$$E_i^u e^{i\Phi_{uu}}(1 + e^{i\Delta\varphi}) = 0 \tag{6}$$

Hence, $\Delta\varphi = \Phi_{uu} - \Phi_{vv} = \pm 180^o + 2k\pi$. Under this condition, the reflected fields in *u*- and *v*-directions (5) will lie along the x-axis.

$$\vec{E}_r = \hat{x}E_r^x = \hat{u}E_r^u - \hat{v}E_r^v \tag{7}$$

Where $E_r^u = E_r^v = E_r^x$. It means that the polarized incident wave is rotated 90 and the converter displays a cross-polarization conversion.

10.22060/EEJ.2026.25702.5991

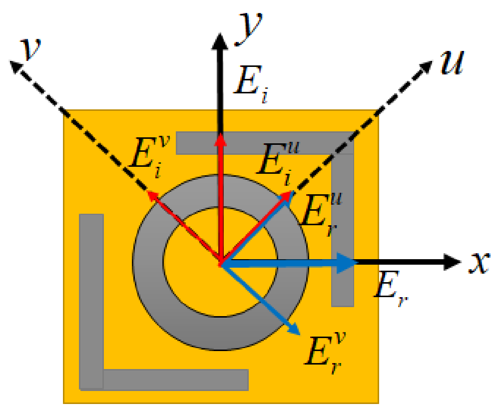

Fig.3 Decomposition of incident y-polarized field into u- and v-components and its conversion into x-polarized wave.

Fig. 4 shows the amplitude of co-polarized reflection coefficients and their phase difference. As observed, the amplitudes of the co-polarized reflection coefficients are nearly equal to 1 for the entire survey frequency range of 4.32 to 13.84 GHz, respectively. Furthermore, the phase difference between the u- and v-components is approximately 180° ± 35°. As reported in [12,37], the excellent polarization conversion ratio can be obtained with a reflection phase difference within the range of 180 + 37° to 180–37°. These results display that the polarization of the EM wave can rotate by a 90○. Therefore, a *y*-polarized incident wave is reflected as an *x*-polarized wave.

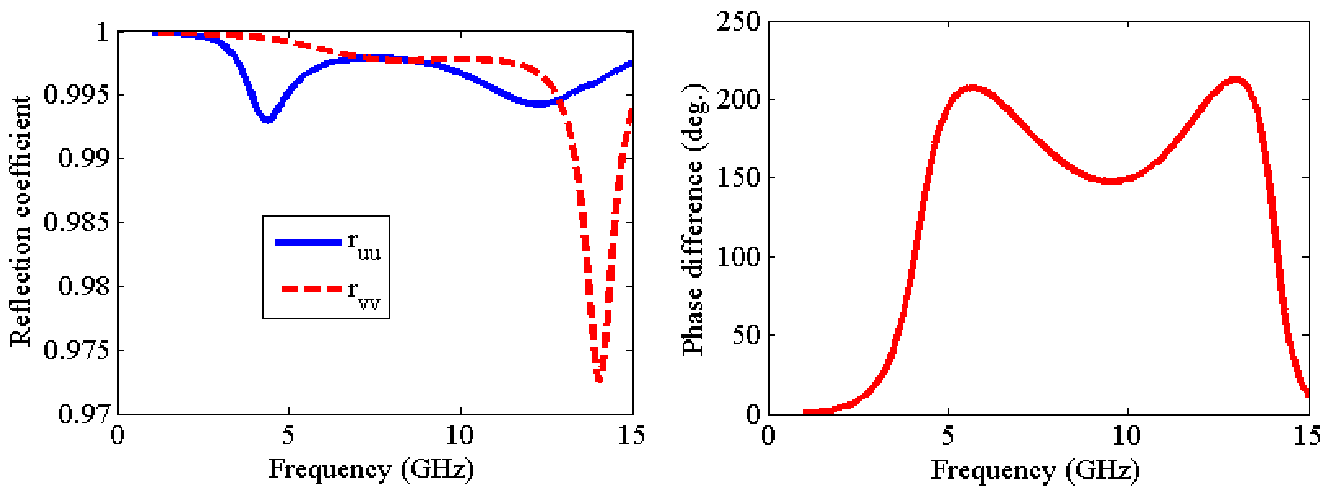

(a) (b)

Fig.4 (a) Amplitude and (b) phase difference of the reflection coefficients of the proposed converter for u- and v-components at the normal incidence.

The effects of dielectric and air spacer thicknesses on the performance of the proposed structure are investigated, as shown in Fig. 5. Increasing the dielectric thickness shifts the polarization conversion band toward lower frequencies and reduces the polarization conversion ratio (PCR). Similarly, as illustrated in Fig. 5(b), variations in the air spacer thickness also influence the PCR, with both increases and decreases leading to a reduction in conversion efficiency. To clarify the design mechanism, a parametric study is carried out by varying the key geometrical parameters of the proposed structure, including the strip length (d), gap spacing (g), and the radii of the circular elements (R_1 and R_2). Fig. 6(a) illustrates the effect of the geometric parameters R_1 and R_2 on the polarization conversion ratio (PCR). It can be observed that the proposed converter maintains broadband polarization conversion for all investigated cases. Among them, the configuration with R_2= 3 mm and R_1= 1 mm provides the most stable response, achieving PCR values close to unity over a wide frequency range. Increasing R_1 slightly shifts the upper resonant frequency and reduces the bandwidth, whereas variations in R_2 have a stronger influence on the response. In particular, R_2 = 4 mm introduces an additional resonance around 11–12 GHz, resulting in a significant reduction in PCR. Therefore, R_2 = 3 mm and R_1 = 1 mm are selected as the optimal dimensions for achieving broadband and high-efficiency polarization conversion. Fig. 6(b) illustrates the influence of the strip length (d) and gap spacing (g) on

10.22060/EEJ.2026.25702.5991

the polarization conversion ratio (PCR). The strip length and gap spacing controls the resonant frequencies, operating bandwidth and PCR values. It is observed that increasing the strip length shifts the resonant frequencies toward lower values due to the increased electrical path length, while variations in the gap spacing modify the electromagnetic coupling between adjacent metallic sections. A smaller gap enhances the coupling strength and shifts the operating band toward lower frequencies, whereas a larger gap provides a smoother PCR response. Based on the parametric analysis, the dimensions d = 10 mm and g = 1 mm are selected as the optimum values for achieving broadband and high-efficiency polarization conversion.

The angular stability of the proposed converter is analyzed in Fig. 7, which presents the PCR as a function of frequency and incident angle up to 40°. The results demonstrate that a PCR above 90% is maintained for incident angles up to 35°, indicating robust angular performance.

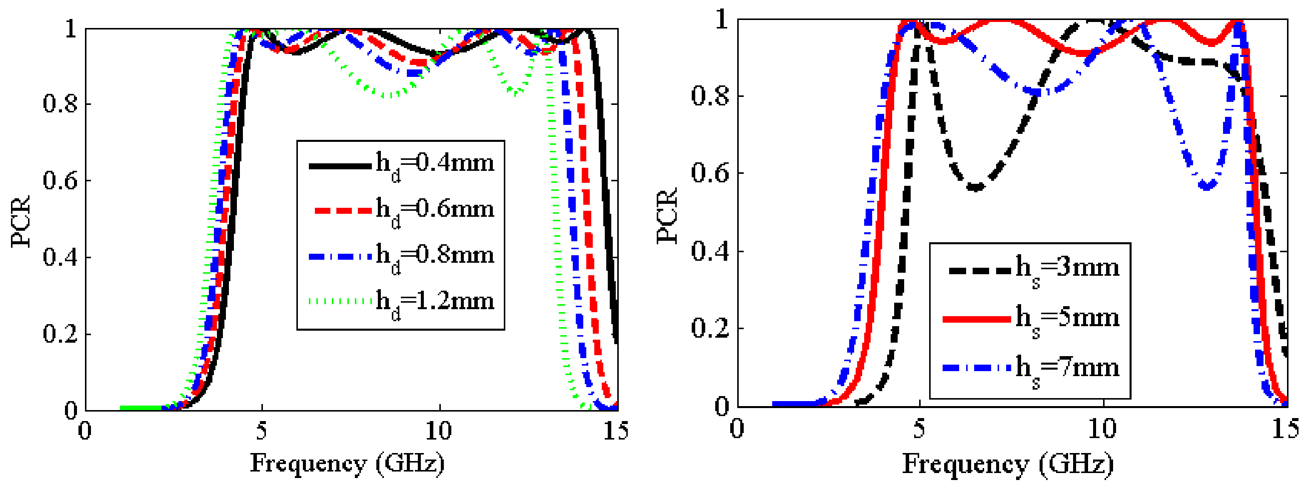

(a) (b)

Fig.5 PCR for various (a) dielectric thickness (b) air spacer thickness for the proposed structure under the normal incidence

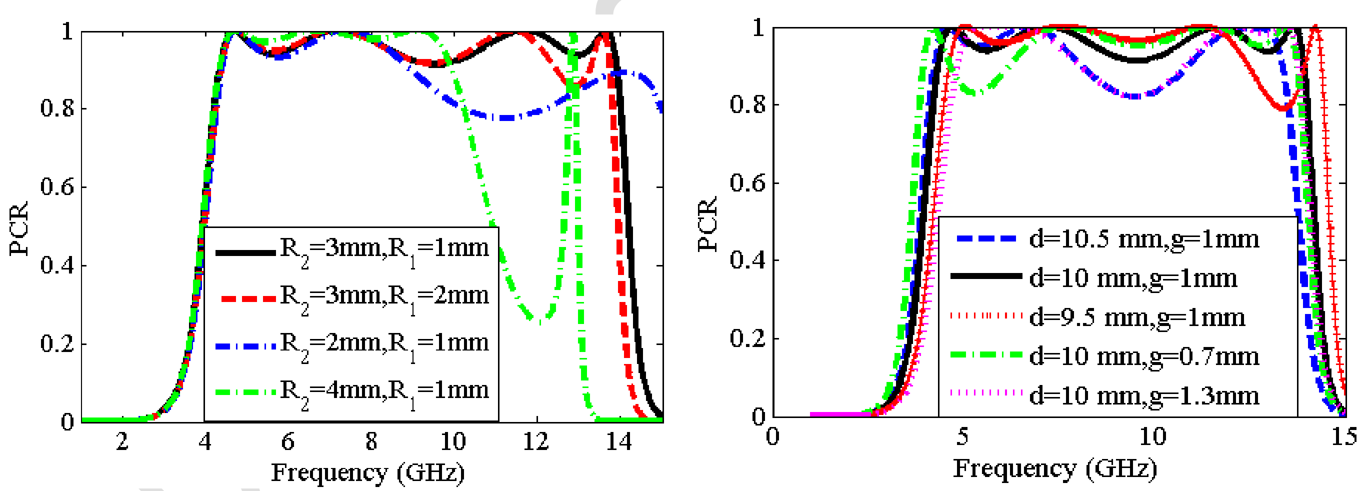

(a) (b)

Fig. 6. PCR of the proposed structure under normal incidence for various values of (a) the circular-element radii (R_1 and R_2) and (b) the strip length (d) and gap spacing (g).

10.22060/EEJ.2026.25702.5991

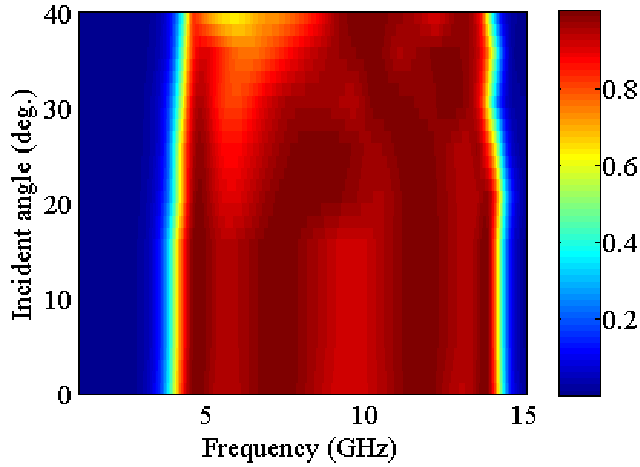

Fig.7 PCR spectra of the proposed structure under the oblique incidence

To elucidate the physical mechanism underlying the broadband polarization conversion, the electric and magnetic field distributions on the metasurface are analyzed at the four resonant frequencies of 4.64, 7.22, 11.64, and 13.65 GHz, as shown in Figs. 8 and 9. At these frequencies, both fields are strongly localized in specific regions of the metasurface. As illustrated, the electric field is primarily concentrated at the edges of the gaps between the two L-shaped metallic strips, whereas the magnetic field is predominantly localized at the central corners and arms of the strips.

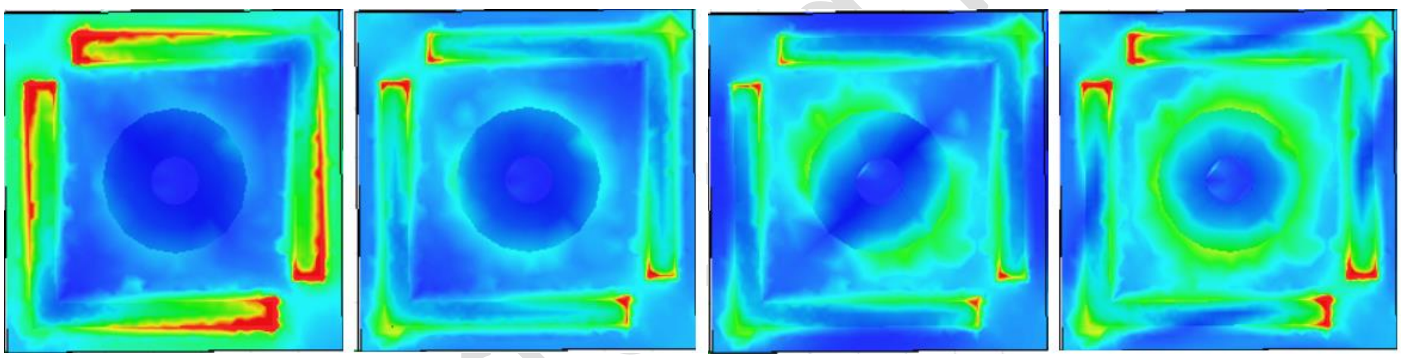
E-Fields

Fig.8 Simulated electric field distributions of the proposed structure at the resonant frequencies, respectively from left to right.

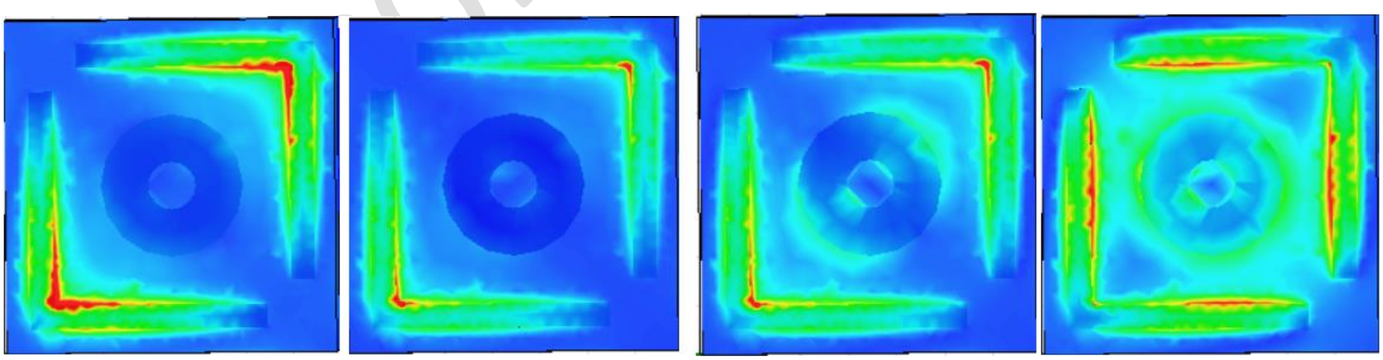
H-Fields

Fig.9 Simulated magnetic field distributions of the proposed structure at the resonant frequencies, respectively from left to right.

The surface current distributions on the top and bottom metallic layers at the four resonant frequencies are presented in Fig. 10. The orientation of the surface currents is indicated by narrow black arrows, highlighting the resonant current paths responsible for the polarization conversion. At the first resonance, the surface currents on the top layer are antiparallel to those on the bottom metallic layer, indicating the presence of a magnetic resonance. In this case, current loops are formed within the intermediate dielectric, characteristic of magnetic resonance. Conversely, at the third resonance, the top and bottom currents are parallel, demonstrating an electric resonance. At the second and fourth resonances, the currents on the top metasurface layer are orthogonal to those on the ground plane, indicating a hybrid response combining both electric and magnetic resonances. These observations confirm that the interplay between electric and magnetic resonances is the primary mechanism enabling ultra-broadband polarization conversion in the proposed metasurface.

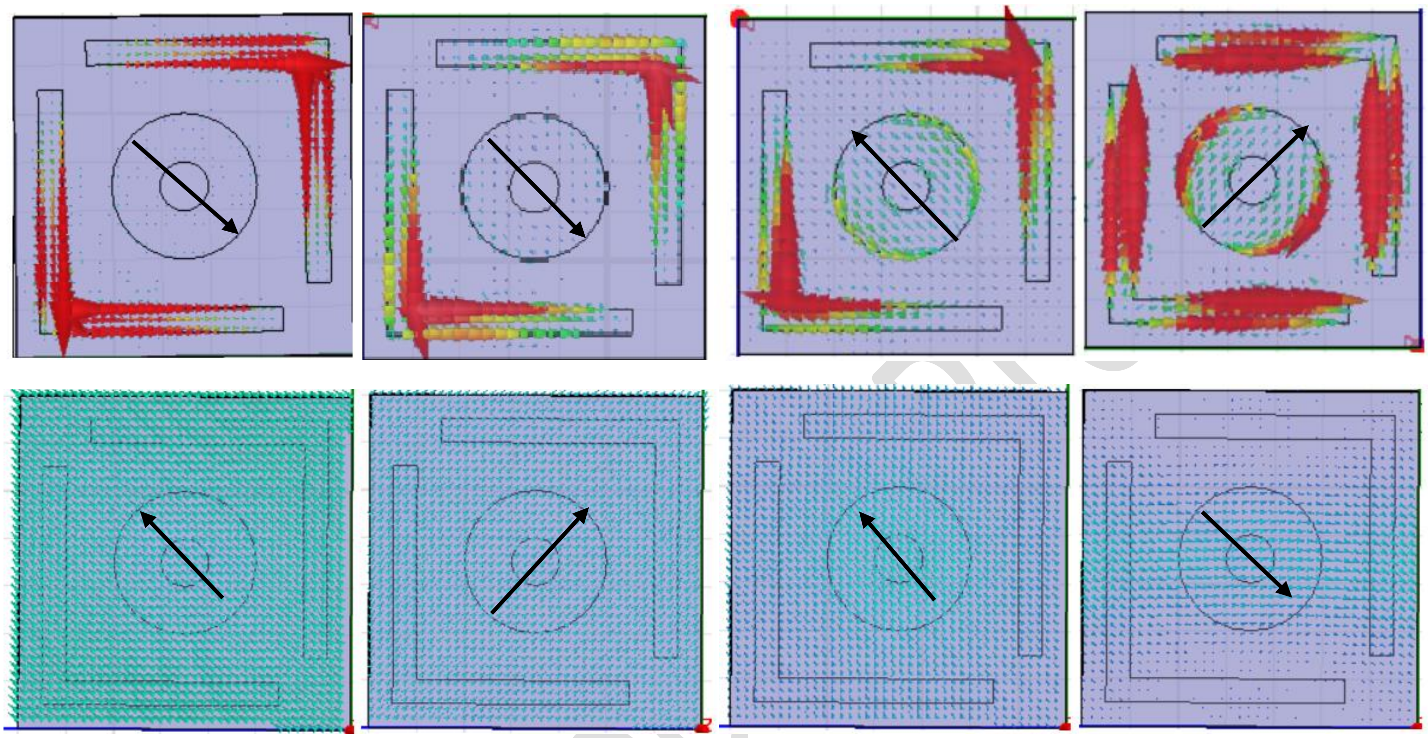

Surface Currents

Fig.10 Surface current distributions on the top and bottom metallic layers of the proposed structure at the resonant frequencies, respectively from left to right. For each case, the upper sub-figures show the current distribution on the metasurface (top layer), while the lower sub-figures present the corresponding distribution on the bottom metallic layer.

The performance of the proposed structure is compared with previously reported polarization converters, and the results are summarized in Table 1. The comparison includes important parameters such as unit-cell configuration, electrical size, substrate thickness, total thickness, angular stability, and operating bandwidth. As shown in Table 1, the proposed polarization converter exhibits a wide fractional bandwidth of 105% (4.32–13.84 GHz), which is comparable to or greater than that of most previously reported designs. Only the structures reported in [10] and [24] achieve slightly larger fractional bandwidths of 111% and 126%, respectively. However, the proposed design offers several notable advantages. Compared with the converter in [10], the proposed structure employs a thinner thickness, resulting in a lower-profile configuration that is more suitable for compact and lightweight microwave systems. Although the design in [24] achieves the widest bandwidth, its operating range is shifted toward considerably higher frequencies (9–40 GHz). In contrast, the proposed converter provides broadband polarization conversion at lower microwave frequencies, which are widely used in radar systems, satellite communications, wireless networks, remote sensing, and electromagnetic compatibility applications. Furthermore, the proposed structure maintains stable polarization conversion performance for incident angles up to 35°, demonstrating good angular robustness. The combination of broad bandwidth, an ultra-thin profile, satisfactory angular stability, and a simple unit-cell geometry based on L-shaped strips and a circular ring highlights the effectiveness of the proposed design. Therefore, the proposed polarization converter offers an attractive balance among bandwidth, profile thickness, angular stability, and structural simplicity, making it a promising candidate for practical broadband polarization conversion applications.

Table. 1 Performance comparison of the proposed structure to other tasks

Ref.	Unit cell of structure	Size of unit cell	Thickness (Dielectric layer)	Total thickness	Angular stability (degree)	bandwidth (GHz)
[10]	A double split ring	14 mm (0.42λ)	1.6 mm (0.048λ)	6.67 mm	30º	4 -14 GHz (111%)
[14]	A fish-like structure	7 mm (0.22λ)	1.6 mm (0.05λ)	1.6 mm	45º	8-11 GHz (31.6 %)
[15]	Double U-shaped metasurface	10 mm (0.35λ)	3 mm (0.106λ)	3.04 mm	-	6.91-14.31 GHz (70 %)
[16]	A oval cut by two metallic strips	12 mm (0.614λ)	2 mm (0.102λ)	2 mm	30º	10.2 - 20.5 GHz (67%)
[18]	Asymmetric double-ring resonators	12 mm (0.476λ)	3.5 mm (0.138λ)	3.54 mm	-	6.67 - 17.1 GHz (87.7%)
[24]	Double-heads arrow	6 mm (0.49λ)	0.25 mm (0.02λ)	2.5 mm	-	9 - 40 GHz (126 %)
[26]	H-shaped metasurface	9.1 mm (0.402λ)	3.5 mm (0.154λ)	3.54 mm	-	7-19.5 GHz (94%)
[27]	Double W-shaped metasurface	6.5 mm (0.36λ)	3 mm (0.167λ)	3.06 mm	40º	8.44 - 24.96 GHz (99%)
This task	L-shaped strips and a metallic circular ring	14 mm (0.42λ)	0.6 mm (0.018λ)	5.64 mm	35º	4.32 -13.84 GHz (105%)

III. CONCLUSION

In this work, a single-layer metasurface-based polarization converter comprising a pair of L-shaped metallic strips and a central circular ring has been proposed for microwave applications. The results confirm that the interaction between electric and magnetic resonances plays a key role in enabling efficient polarization manipulation and sustaining broadband operation. The proposed structure exhibits efficient cross-polarization conversion over a wide frequency range of 4.32–13.84 GHz, with a polarization conversion ratio (PCR) exceeding 90% and angular stability up to 35°. In addition to the demonstrated performance, the proposed design offers strong potential for practical implementation in modern electromagnetic systems. Its compact, planar, and low-profile configuration makes it suitable for integration into antenna systems, where it can enhance polarization purity, improve radiation efficiency, and enable polarization diversity. In radar and sensing applications, it can reduce polarization mismatch and improve detection reliability under varying incidence conditions. Furthermore, its wide-angle response and stable performance indicate suitability for satellite and wireless communication systems requiring robust operation under oblique incidence. It may also find applications in stealth technology and electromagnetic compatibility (EMC) engineering, where controlled polarization conversion is important for managing scattering and interference. Overall, the proposed design combines structural simplicity with functional versatility, offering a promising solution for next-generation polarization control devices requiring broadband and wide-angle performance in practical microwave systems.

Declarations

Competing Interests The authors declare that they have no known competing financial interests or personal relationships that could have appeared to influence the work reported in this paper.

10.22060/EEJ.2026.25702.5991

REFERENCES

[1] G. Chaitanya, P. Peshwe, S. Ghosh, A. Kothari "Design of bandwidth-enhanced polarization controlled frequency selective surface based microwave absorber" *International Journal of Microwave and Wireless Technologies*., 16 (5) (2024), 862-870.

[2] J. Chen, Y. Shang, and Ch. Liao, "Double-Layer Circuit Analog Absorbers Based on Resistor-Loaded Square-Loop Arrays," *IEEE Antennas and Wireless Propagation Letters*, 17(4) (2018) 591-595.

[3] C. Barde, NK. Gupta, P. Ranjan, K. Roy, R.Sinha, "Angle-independent wideband metamaterial microwave absorber for C and X band application," *International Journal of Microwave and Wireless Technologies.*, 16(1) (2024), 101–109.

[4] I. V P, S. V P, V. C and S. Kumar T R, "Design of Broadband Circuit Analog Absorber With Optimal Thickness for Stable Angular Response in C, X, Ku, and K Bands," *IEEE Transactions on Electromagnetic Compatibility*, 65(6) (2023), 2065-2069.

[5] S. Zhao, W. Li, Z. Li, H. Shu, K. Qi, H. Yin, "Ultra-Broadband Absorber with Large Angular Stability Based on Frequency Selective Surface," *Materials*, 15 (2022) 6452.

[6] S. Barzegar-Parizi, "Circuit Analog Absorber Based on a Double-Layer of Resistor-Loaded Strip Arrays with Various Bandwidths according to Selecting the Polarization," *Journal of Electrical and Computer Engineering Innovations*., 13 (2) (2025) 299-306.

[7] S. Barzegar-Parizi, Z. Vafapour, "A switchable polarization-independent broadband GST-based metasurface infrared absorber in modulating applications," *Appl. Phys. A*., 129 (2023), 790.

[8] M. Zhang, B. Zhang , X. Liu, Sh. Sun, and Ch. Jin, "Design of Wideband Absorber Based on Dual-Resistor-Loaded Metallic Strips," *International Journal of Antennas and Propagation.*, 2020 (2020), Article ID 1238656, 1-8.

[9] S. Ghosh, K. V. Srivastava, and S. Bhattacharyya, "Design, characterization and fabrication of a broadband polarization insensitive multi-layer circuit analogue absorber," *IET Microwaves, Antennas & Propagation*, 10 (8) (2016), 850–855.

[10] T. M. Nguyen, H. L. Phan, D. L. Vu, T. Q. H. Nguyen, J.-M. Kim, "Ultra-wideband and high-efficiency cross-polarization conversion using a double split ring shaped metasurface for C, X, and Ku band applications," *AIP Advances*., 12 (2022), 115002.

[11] M. I. Khan, Q. Fraz, and F. A. Tahir, "Ultra-wideband cross polarization conversion metasurface insensitive to incidence angle," J. Appl. Phys., 121 (2017), 045103.

[12] Z. Zhang, J. Wang, X. Fu, *et al.* "Single-layer metasurface for ultra-wideband polarization conversion: bandwidth extension via Fano resonance," *Sci Rep*., 11 (2021), 585.

[13] M. I. Khan, Sh. A. Khan Tanoli, F. A. Tahir and B. Hu, "Multiband linear and circular polarization converting anisotropic metasurface for wide incidence angle," *J. Phys. D: Appl. Phys*., 53 (2020), 095005.

[14] M. I. Khan, Z. Khalid, and F. A. Tahir, "Linear and circular-polarization conversion in X-band using anisotropic metasurface" *Sci Rep.*, 9 (2019), 4552.

[15] Zh. L. Mei, X. M. Ma, C. Lu, and Y. D. Zhao, "High-efficiency and wide-bandwidth linear polarization converter based on double U-shaped metasurface," *AIP Advances.*, 7 (2017), 125323.

[16] M. Karamirad, C. Ghobadi and J. Nourinia, "Metasurfaces for Wideband and Efficient Polarization Rotation," *IEEE Transactions on Antennas and Propagation*, 69(3) (2021), 1799-1804.

[17] H. Yu, X. Wang, J. Su, M. Qu, Q. Guo, Z. Li, and J. Song, "Ultrawideband and high-efficient polarization conversion metasurface based on multi-resonant element and interference theory," *Opt. Express.*, 29 (2021), 35938-35950.

[18] J. Xu, R. Li, Sh. Wang, and T. Han, "Ultra-broadband linear polarization converter based on anisotropic metasurface," *Opt. Express.*, 26 (2018), 26235-26241.

[19] B. Khan, B. Kamal, S. Ullah, *et al.* "Design and experimental analysis of dual-band polarization converting metasurface for microwave applications," *Sci Rep*., 10 (2020), 15393.

[20] U. R. Qureshi, B. Hu, Sh. Basir, M. Ahmad, A. Jalal and M. I. Khan, "Design and experimental realization of multifunctional anisotropic metasurface for efficient polarization manipulation in microwave frequencies," *Phys. Scr.*, 99 (2024), 015512.

[21] Y. Zheng, Y. Zhou, J. Gao, *et al.* "Ultra-wideband polarization conversion metasurface and its application cases for antenna radiation enhancement and scattering suppression," *Sci Rep*., 7 (2017),16137.

[22] Y. Jiang, M. Li, J. Wang, X. Huang, S. A. Zhang, "Metamaterial-Based Cross-Polarization Converter Characterized by Wideband and High Efficiency," *Crystals.*, 13(2023).

[23] M. S. Wahidi; Meraj-E- Mustafa; F. A. Tahir, "Comment on "An ultrathin and broadband metamaterial absorber using multi-layer structures" [J. Appl. Phys. 114, 064109 (2013)]," *J. Appl. Phys.*, 125 (2019), 166101.

[24] E. Ameri, S. Esmaeli, S. Sedighy, "Ultra Wideband Radar Cross Section Reduction by Using Polarization Conversion Metasurfaces," *Sci Rep*, 9 (2019), 478.

[25] S. Sun, W. Jiang, X. Li, P. Liu and S. Gong, "Ultrawideband High-Efficiency 2.5-Dimensional Polarization Conversion Metasurface and Its Application in RCS Reduction of Antenna," *IEEE Antennas and Wireless Propagation Letters*, 18(5) (2019), 881-885.

10.22060/EEJ.2026.25702.5991

[26] J. Xu, R. Li, J. Qin, Sh. Wang, and T. Han, "Ultra-broadband wide-angle linear polarization converter based on H-shaped metasurface," *Opt. Express.*, 26 (2018), 20913-20919.
[27] Y. Zhao, B. Qi, T. Niu, Zh. Mei, L. Qiao, and Y. Zhao, "Ultra-wideband and wide-angle polarization rotator based on double W-shaped metasurface," *AIP Advances.,* 9 (2019), 085013.
[28] Z. X. Wang, and J. F. Wang, "Multi-octave RCS reduction via integrated dispersion engineering of polarization-conversion metasurface and metamaterial absorber," *J. Phys. D Appl. Phys.*, 53 (3) (2019).
[29] Y. Cheng, J. Fan, H. Luo, F. Chen, N. Feng, X. Mao, and R. Gong, "Dual-band and high-efficiency circular polarization conversion via asymmetric transmission with anisotropic metamaterial in the terahertz region," *Opt. Mater. Express*., 9(2019), 1365-1376.
[30] A. Majeed, Zh. Jinling, H. A. Khan, M. Ishfaq, B. Hayat, "Multiband dual polarization conversion metasurface based on three-quarter circular-shape in the terahertz regime," *Results in Physics*, 57 (2024), 107398.
[31] T. Meissner and F. J. Wentz, "Polarization rotation and the third stokes parameter: the effects of spacecraft attitude and faraday rotation," *IEEE Trans. Geosci. Remote Sens*., 44(3) (2006), 506–515.
[32] J. Xu, T. Li, F. F. Lu, S. M. Wang, and S. N. Zhu, "Manipulating optical polarization by stereo plasmonic structure," *Opt. Express.,*19(2) (2011), 748–756.
[33] M. Mutlu and E. Ozbay, "A transparent 90° polarization rotator by combining chirality and electromagnetic wave tunneling," Appl. Phys. Lett., Vol. 100(5), p. 051909, 2012.
[34] S. S. Pati, S. Sahoo, "Single/Dual/Triple Broadband Metasurface Based Polarisation Converter with High Angular Stability for Terahertz Applications," *Micromachines*, 13(9) (2022), 1547**.**
[35] B. Kamal, J. Chen, Y. Yingzeng, J. Ren, S. Ullah, and W. Ur Rehman Khan, "High efficiency and ultra-wideband polarization converter based on an L-shaped metasurface," *Opt. Mater. Express.,* 11 (2021), 1343-1352.
[36] S. Barzegar-Parizi, "Dual functional Device Featuring Absorption and Polarization Conversion Based on Temperature Controlled Metasurface for Terahertz Applications," *Sci Rep*., 16 (2026), 20858.
[37] T. N. Cao, M. T. Nguyen, N. H. Nguyen, Ch. L. Truong and T. Q. H. Nguyen, "Numerical design of a high efficiency and ultra-broadband terahertz cross-polarization converter," *Mater. Res. Express*., 8 (2021), 065801.